Applied Chemistry Today **19(73)** (2024) 155-168

Semnan University

Applied Chemistry Today

Journal homepage: https://chemistry.semnan.ac.ir/

ISSN: 2981-2437

Research Article

Electrode Potential for a Series of Oligo(pyrrole)s: Theoretical and Experimental Approaches

Zeynab Ashrafi[a], Hossein Nikoofard[a,*], Mobina Hosseni[b]

[a]*Faculty of Chemistry, Shahrood University of Technology, Shahrood 36199-95161, Iran*

[b]*School of Chemistry, Damghan University, Damghan 36716-41167, Iran*

PAPER INFO

Article history:
Received: 04/Jul/2024
Revised: 14/Sep/2024
Accepted: 14/Sep/2024

Keywords:
Oligo(pyrrole);
DFT calculations;
Cyclic voltammetry;
Oxidation potential;
IV-curves.

ABSTRACT

The study of oxidation potential and electronic properties of conducting polymers are very important for designing new material with improved properties. The current study focused on the electrochemical information about potential electrode of pyrrole (Py) oligomers, *n*Py: *n* = 2-8, as well as their structural and electronic properties. Computational chemistry based on DFT calculations were used to determine an accurate standard oxidation potential (E_{ox}°) for the *n*Py with respect to the calomel reference electrode in the aqueous and non-aqueous solutions. A nice agreement between the predicted and available experimental redox potential was obtained with an average absolute deviation of 0.016 V. A good linear correlation with both the HOMO level and the ionization potential were obtained for the E_{ox}° values. Additionally, an estimated E_{ox}° value of 0.21 V vs. SCE was obtained for poly(Py) in THF. The simulated current-voltage (IV) curves revealed an increase in the conductivity of *n*Py chains as the length of oligomer increasing. Based on the analysis of the band gap from the TD-DFT spectral results, a high ease of charge transport was observed for long oligomer chains. Poly(Py) films were synthesized electro-chemically by the direct anodic oxidation of pyrrole in an aqueous solution via cyclic voltammetry (CV) technique. It was found that the oxidation potential for oligo(Py) chains decreases through the growing polymer during the electro-polymerization.

DOI: https://doi.org/10.22075/chem.2024.34471.2281

[*] **.corresponding author:** Associate Professor of Physical Chemistry. *E-mail address: hnikoofard@shahroodut.ac.ir*

How to cite this article: Ashrafi, Z., Nikoofard, H. & Hosseini, M. (2024). Electrode Potential for a Series of Oligo (pyrrole) s: Theoretical and Experimental Approaches. *Applied Chemistry Today*, **19(73)**, 155-168. (in Persian)

1. Introduction

The investigation of the electronic, optical, and magnetic characteristics of conjugated polymers was initiated in the 1970s following the identification of poly(acetylene) as conducting polymer by Shirakawa et al. [1]. The chemical and electro-chemical synthesis of π-conjugated organic materials and the subsequent success in their doping to create the electrical conducting materials established the field of conducting polymers. These kinds of polymers are widely used for industrial applications such as solar cells [2, 3], light emitting diodes (LEDs) [4, 5], electrochromic devices [6, 7], gas sensors [8-10] and field effect transistors [11]. An electrochromic material sustains reversible and persistent changes of its optical properties upon applied potential. The acknowledgment of the Nobel Prize for chemistry in the year 2000, bestowed upon Heeger, MacDiarmid, and Shirakawa, served to validate the significance of the identification and advancement of conductive polymers [12]. Among the conducting materials, Py-containing polymers have various useful properties such as high charge carrier mobility, high photochemical and thermal stability [13, 14].

By convention, Py derivatives have a unique mechanism for polymerization process which is depicted in Scheme 1 [15]. In the first step (a), a Py monomer in its neutral form (ground state) undergoes a one-electron oxidation reaction to generate a radical cation form (oxidized state). In the subsequent step (b), the acquired radical cation can engage in recombination with another radical cation to form a dihydro-dication (c); this process can be followed by the elimination of two protons resulting in the production of a neutral bi-Py molecule as a dimer (d). The neutral dimer has the potential to undergo an additional oxidation process (recombination and deprotonation steps), leading to large oligo(Py) chain and, consequently, poly(Py) as the final product. The properties associated with the oxidation reaction of Py and oligo(Py)s serve as an effective indicator of reactivity for the coupling reaction, thereby facilitating the formation of desirable conducting materials. The electro-chemical experiments were shown that the oxidation potential of oligomeric chains of Py are lower than its monomer due to a higher degree of π-conjugation, more charge delocalization, and the planarity of the backbone chain [16]. However, most of the experiments deal with electro-chemical characterization of the conducting polymer for immediate applications, precise information about exact values of oxidation potentials for oligomers is quite scarce.

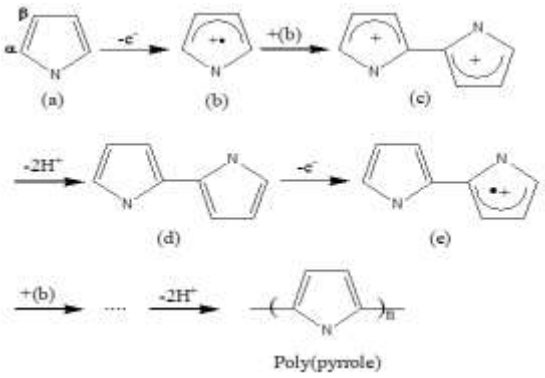

Scheme 1. A unique mechanism for electro-polymerization of Py monomer [15].

During the last decades, a great number of theoretical and experimental studies have provided important information about the structural and opto-electronic properties of the conjugated oligo- and polymer species, contributing to their remarkable electrical and optical features [17-19]. In this regard, a fundamental challenge is to develop consistent, instructive, and computationally efficient theoretical methodologies for the estimation of oxidation potential as a conduction property. In the current work, an alternative method of calculations is presented in order to predict the electrode potential of the nPy species including n = 2(di), 3(tri), 4(tet), 5(pen), 6(hex), 7(hep), and 8(oct) building units of oligomer chain in the gas phase and both water and

tetrahydrofuran (THF) solutions. A comparative analysis has been undertaken to evaluate the findings acquired in this study with those that were previously reported. The investigation was extended by analysing the first stages of poly(Py) electro-synthesis by cyclic voltammetry (CV) measurements [20].

2. Methodology

2.1. Experimental method

A standard three-electrode cell was used with a glassy carbon (GC) disk as the working electrode, a saturated calomel electrode (SCE) as reference, and a platinum wire as the counter electrode. Before each experiment, the working electrode was polished mechanically with 1.0 mm diameter alumina powder, washed, and then rubbed against a smooth cloth. All the electro-chemical measurements were carried out using the electro-chemical system AMEL instrument (Italy) with a PC and electro-chemical set-up that was controlled with the software. Pyrrole (Merck) was distilled under reduced pressure before use. Deionized water from a Millipore purification system was used for the preparation of the solutions. All the experiments were carried out in a supporting electrolyte containing KNO_3 (0.2 M) at room temperature.

2.2. Computational details

The density functional theory (DFT) has been found as one of the most favorable techniques of theory for responsible and precise calculations at minimum cost for macromolecule system [21, 22]. All calculations were done using the B3LYP/6-31G(d,p) level of theory as implemented in the Gaussian 09 suite of the program [23]. The initial geometry optimization of all structures in both the ground and oxidized states was carried out in the water and THF solvents as well as the gas phase. The solvation Gibbs free energy calculations in the condensed phase were done via the conductor-like polarizable continuum model (CPCM) [24]. Following the geometry optimization, the TD-DFT formalism [25] from both the ground and oxidized structures of each oligo(Py) at TD/B3LYP/6-31G(d,p) level of theory was used to calculate the excited states to achieve simulated UV-vis spectra. The IV-curves have been simulated for the short oligomer chains using Quantumwise Atomistix Toolkit (ATK) simulator [26, 27].

3. Result and discussion

3.1. Molecular structure

The mean dihedral angle (Δ), defined by torsional angle between two adjacent Py monomer ring along the oligo(Py) backbone, in the gas phase and the water solvent are given in Table 1. Calculation results indicate that the mean dihedral angles for the ground state oligomers are changed in 22.7°-26.8° in the gas phase. In other words, all oligomer chains are away from the planarity backbone (0°), decreasing when the oligomer chain increased. According to Table 1, in the case of oxidized states, the torsional angles decreases significantly up to 0◦. It means that the excess charge induced a geometric distortion generating a planar structure. It is known that the planarity of oligomer backbone, and thereby, final polymer is an important key factor in their electrical conduction. When solvation effects are introduced, the mean dihedral angle for the ground states (column 3) decreased about 7.3° with respect to ones in the gas phase while it remains unchanged ($\approx$ 0°) in the oxidation forms (column 6).

Table 1. The mean dihedral angles (in degree) along the oligomer chains in the gas phase and water solution

	Δ Ground state		Δ Oxidized state	
Oligo(Py)s	gas	water	gas	water
di(Py)	26.8	19.5	0.0	0.0
tri(Py)	24.5	15.6	0.0	0.0
tet(Py)	23.3	16.1	0.0	0.0
pen(Py)	21.9	15.1	0.0	0.0
hex(Py)	22.8	15.6	0.0	0.0
hep(Py)	22.5	15.7	2.1	1.3
oct(Py)	22.7	15.4	3.9	2.3

The parameter denoted as the bond length alternation (δ) is a significant factor that is associated with the π-conjugation of a molecule [28]. In this context, it is defined as follows:

$$\delta = 2r_{\beta\beta'} - (r_{\alpha\beta} + r_{\alpha'\beta'}) \quad (1)$$

where $r_{\beta\beta'}$, $r_{\alpha\beta}$, and $r_{\alpha'\beta'}$ denote the mean single C(β)-C(β′) and the double C(α)=C(β) and C(α′)=C(β′) bonds along the backbone oligo(Py) chain, respectively (as being labelled in Scheme 1). The δ values with the mean single and double bond lengths ($\bar{r}_{C-C}$ and $\bar{r}_{C=C}$) for each oligo(Py) chain were calculated in both the ground and oxidized states, which was quoted in Table 2.

Table 2. The alternation parameter (Å) for the ground and oxidized states of oligo(Py)s in water solvent.

Oligo(Py)s	δ Ground state	δ Oxidized state
di(Py)	0.0467	-0.0239*
tri(Py)	0.0438	-0.0094
tet(Py)	0.0423	-0.0008
pen(Py)	0.0413	0.0047
hex(Py)	0.0406	0.0090
hep(Py)	0.0403	0.0123
oct(Py)	0.0399	0.0162

* The term (-) pertains to a quinoid structure in which the inter-ring bond has a greater double bond character than that in the conventional aromatic configuration.

It is clear that a quantity of δ value closer to the zero ($\delta \rightarrow 0$) corresponds to an increase in the aromatic character of C-C bonds along the conjugated polymer chain. In this regard, for all oligo(Py)s, the bond alternation parameter in the oxidized state was lower remarkably than those in the ground states in the range of 0.0029–0.0081 Å. It has been determined that a small value of the bond length alternation could potentially be indicative of an improved π-conjugation system, the narrow gap energy between the highest occupied molecular orbital (HOMO) and the lowest unoccupied molecular orbital (LUMO), as well as a low value of excitation energy. One can also see in Table 2, in the case of ground states (column 4), the δ value depended on the oligomer chain, decreasing slightly under the propagation step of the polymerization mechanism (Scheme 1). It was concluded that the increasing of the oligomer chain leads to enhance the conjugation length of the backbone of the final poly(Py).

3.2. Electronic properties

It is convenient to investigate the HOMO and LUMO for the title oligomers because the relative ordering of the occupied and virtual orbitals provides a reasonable qualitative indication of the excitation properties and of the ability of electron or hole transport. Delocalization of the π-electrons across the molecular structure leads to a satisfactory resonance system, which associated with a narrow HOMO-LUMO gap (HLG). As previously stated, this quantity can offer a meaningful qualitative indication of the properties of excitation and the capability of charge transport. The HOMO, LUMO, and HLG values for all oligo(Py)s in both the ground and oxidized states are tabulated in Table 3. In all cases, the energy of the highest occupied molecular orbital escalates as the chain length of oligomer increases while the energy of the lowest unoccupied molecular orbital diminishes due to increase in the extent of conjugation. Consequently, this results in a reduction in HLG which is one of the requirements for enhanced electrical conductivity. As shown in Table 3, the HLG values for the oxidized species (0.031-0.054 eV) are less than those for the corresponding the neutral species (0.120-0.184 eV). The oxidation process of oligo(Py)s destabilizes both the HOMO and LUMO levels. This exhibits an increase in the HOMO and a decrease in the LUMO levels of oligo(Py)s, after the oxidation reaction, and then a reduction value for the HOMO-LUMO energy gap. It was found that the growth of oligomer chain led to a slight decrease in HLGs, thereby, one may find that the final polymer consisting of the Py units possesses a higher electrical conductivity than each oligo(Py).

The analysis of the HOMO-LUMO topological characteristics holds great significance in elucidating the kinetic stability, and by extension, the potential chemical reactivity, along with other attributes like optical properties [29]. In the case of pen(Py) chain, n = 5, in both the ground and oxidized states, the HOMO and LUMO distribution patterns are illustrated in Fig. 1. As one can see in Fig. 1, all the involved HOMO orbitals have π-bonding character which extends on the double C(α)=C(β) and C(α′)=C(β′) bonds along the oligomer chain in both the ground and oxidized states. In the case of LUMO, it possesses an anti-bonding character (π^*) spared mostly over the joint Py-rings related to the ground state while exhibiting a π-character generally in the oxidized state.

Table 3. HOMO, LUMO, and energy gap (eV) for oligo(Py)s in water solvent.

	Ground state			Oxidized state		
Oligo(Py)s	HOMO	LUMO	HLG	HOMO	LUMO	HLG
di(Py)	-0.179	0.005	0.184	-0.228	-0.283	0.054
tri(Py)	-0.166	-0.010	0.156	-0.200	-0.146	0.053
tet(Py)	-0.159	-0.018	0.141	-0.185	-0.144	0.041
pen(Py)	-0.155	-0.022	0.132	-0.176	-0.136	0.040
hex(Py)	-0.153	-0.025	0.127	-0.170	-0.134	0.036
hep(Py)	-0.151	-0.027	0.124	-0.166	-0.133	0.033
oct(Py)	-0.150	-0.029	0.120	-0.164	-0.132	0.031

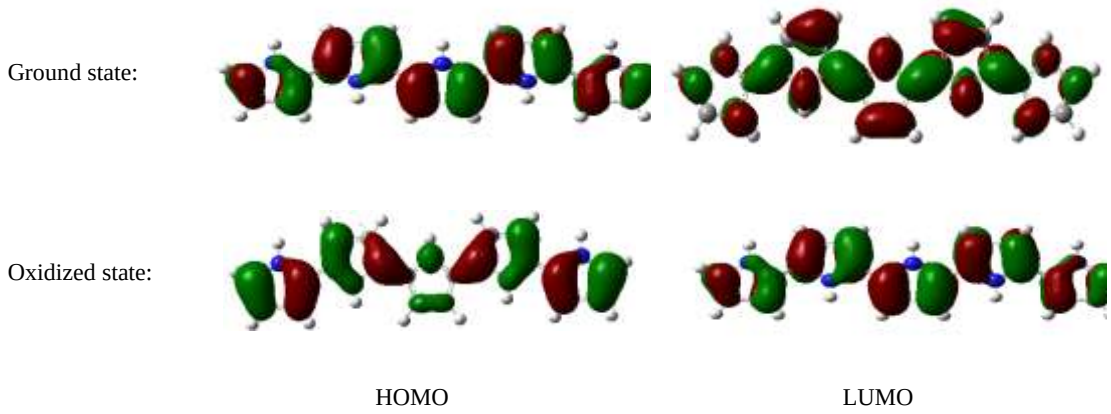

Fig. 1. Diagrams of HOMO and LUMO for the pen(Py) chain in both the ground and oxidized states.

It is evident that the creation of intermediate radical cations from the neutral states plays a significant role in the polymerization process of conductive polymers (Scheme 1). This process can be interpreted as an ionization reaction. The adiabatic ionization potential (IP) is closely corresponded to the degree of electron extraction (or hole injection) to form p-type semi-conductors. The efficient injection and transportation of both holes and electrons are crucial factors for the rational design of optimized light emitting diodes, resulting in the commendable performance of conductive polymers in devices like organic light emitting diodes (OLEDs). Electronic energies for the ground and oxidized states of the oligo(Py)s obtained from the optimized structures at the B3LYP/6-31G(d,p) level of theory, were used to calculate the adiabatic IP in the gas and condensed phases. In Table 4, the IP quantity, as an important parameter for estimating the energy barrier for the injection of holes into the backbone of molecule, indicates a decrease with increase in the conjugated length of oligomer. In other words, as the oligomer chain length increases, the IP values decrease, corresponds to improvement in the hole injection properties. This observation is likewise in line with the pattern of changes in the

case of HLG values. In general, it may be concluded that a lower applied potential requires for propagation step of the polymerization process. This prediction is in agreement with the lower oxidation potential measured experimentally [30, 31].

Table 4. Predicted values of ionization potential (IP) for Py monomer and oligomers (in eV) in different media.

Species	gas	water	THF
monomer	0.287	0.205	0.215
di(Py)	0.235	0.169	0.177
tri(Py)	0.212	0.155	0.162
tet(Py)	0.199	0.149	0.155
pen(Py)	0.191	0.145	0.151
hex(Py)	0.186	0.143	0.148
hep(Py)	0.181	0.142	0.147
oct(Py)	0.178	0.138	0.146

As one can be seen from Table 4, the ionization potential energies are quite similar for the oligo(Py)s in both the aqueous and non-aqueous solutions, which is lower than those in the gas phase. It is revealed that the solvation process is more favorable for the electro-polymerization of pyrrole derivatives in present a condensed phase. For all the studied species, the observed trend is ordered as $IP_{water} < IP_{THF} < IP_{gas}$.

3.3. Electro-chemical properties

For designing new conducting materials with improved properties and possible technological applications, it is necessary to know about electro-chemical behavior of monomer and its oligomers. Electro-chemical synthesis of poly(Py) was performed by the CV method from the solution of Py monomer (0.07 M) in KNO_3 (0.2 M) on a GC electrode using a potential sweep rate of 100 mVs^{-1} between -1 and +1 V (Fig. 2). The CVs exhibited an anodic oxidation peak (I_{pa}) at ca. +0.7 V, which could be attributed to the oxidation of the Py monomer to the radical cation and then to the dication. The absence of a reverse cathodic peak can be attributed to a fast follow-up chemical reaction following the oxidation of the monomer [34, 35]. During the second forward scan, a new anodic peak was observed less than +0.7 V, which corresponds to the reversible oxidation of the oligomeric products of Py. The growth/deposition of the poly(Py) film on the electrode surface was observed by monitoring the CVs during the subsequent scans. A considerable increase in I_{pa} at around 0.2 V is related to the oxidation of the poly(Py) film. It is clear from the figure that the oxidation peaks current for oligo- or poly(Py) in all cycles increases through the electro-chemical polymerization.

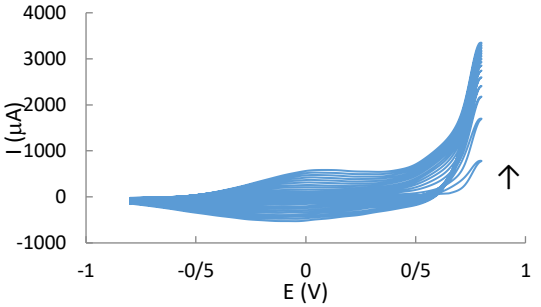

Fig. 2. CVs for polymerization of Py (0.07 M) in KNO_3 aqueous solution (0.2 M) on GCE at scan rate of 100 mV s^{-1}.

The direct proportionality of the amount of polymer to the positive peak current is fundamentally important for studying the Py electro-polymerization. Fig. 3 compares the 1th and 15th cycle numbers of voltammograms of electro-synthesis of 0.07 M monomer. It is an important feature that the layer-by-layer growth mode demonstrates the electro-chemical feasibility of ultrathin polymer films, where these ultrathin films play an important role in different applications.

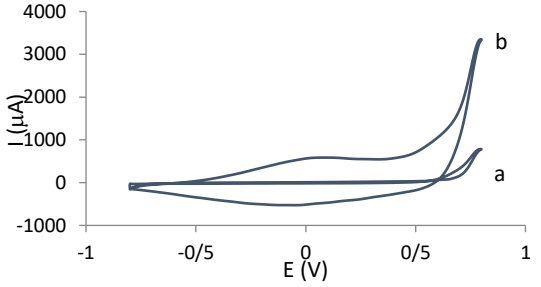

Fig. 3. Comparison of 1th (a), and 15th (b) cycles of CVs for polymerization in 0.07 M Py/0.2 M KNO3 aqueous solution on GCE at scan rate of 100 mV s^{-1}.

Based on CVs of the polymerization process of Py (see Fig. 2), there is a noticeable trend towards lower potential values for oxidation of Py derivatives as the cycle number increases. In this regard, the half-

wave potential ($E_{1/2}$), defined the potential to reach current that equals to half-value of diffusion-limited current, was plotted against the number of cycles for CVs in Fig. 4. It was observed that as the number of cycles increased, a lower $E_{1/2}$ value was obtained. In other words, the potential needed for the oxidation of Py products decreased with an increase in the number of cycles. This behavior is anticipated because as the polymer film grows, the length of the π-electron conjugated system along the polymer chains increases, resulting in a decrease in the energy required for its oxidation.

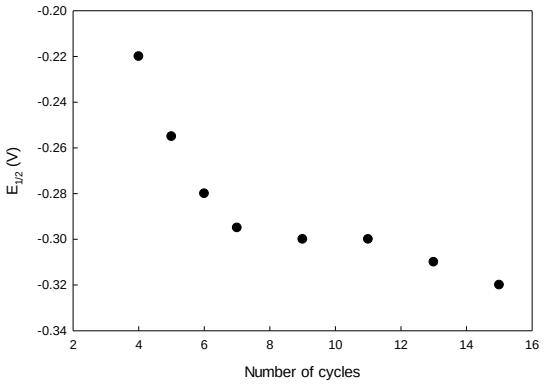

Fig. 4. The half-wave potential ($E_{1/2}$) against the number of cycles for CVs of Py polymerization in 0.07 M Py/0.2 M KNO_3 aqueous solution on GCE at scan rate of 100 mV s^{-1}.

The quantum chemical calculations offer suitable tools capable of predicting the redox potential. By convention, the reduction potential reveals the tendency of a chemical species to gain electrons and thereby, be reduced, in which it is the inverse of the oxidation potential. Here, we consider the following one-electron half-oxidation reaction for the first step of electro-polymerization mechanism (Scheme 1) in the present solvent:

$$Red(sol) \rightarrow Ox^{+\bullet}(sol) + e^- \quad (1)$$

where Red, and $Ox^{+\bullet}$ denote the ground and oxidized states of Py or oligo(Py), respectively. The thermochemical characteristics of Eq. (1) can be employed to ascertain the oxidation potential (E_{ox}). In relation to this matter, in order to compute the standard oxidation potential of each oligo(Py), it becomes imperative to determine the standard free energy change (ΔG^o) for the oxidation reaction (Eq. 1). ΔG^o is related to the standard oxidation potential via the subsequent thermodynamic expression:

$$E_{ox}^{\circ} = -\frac{\Delta G^{\circ}}{nF} \quad (2)$$

where n is the number of electrons transferred in the reaction (it is equal to one in this case) and F is the Faraday's constant (23.061 kcal $mol^{-1}V^{-1}$). To calculate ΔG^o, one can use the thermodynamic cycle in solution [32], as depicted in Scheme 2.

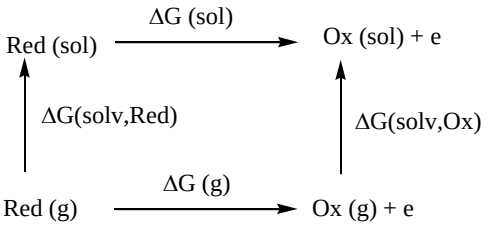

Scheme 2. Thermodynamic cycle for predicting redox potentials in solution.

According the thermodynamic cycle in Scheme 2, ΔG^o of reaction 1 can be written as:

$$\Delta G^o = \Delta G^o(g) + \Delta G^o(solv,Ox) - \Delta G^o(solv,Red) \quad (3)$$

where $\Delta G^o(g)$ is the change in the standard free energy of the oxidation reaction in the gas phase, and $\Delta G^o(solv,Ox)$ and $\Delta G^o(solv,Red)$ are the standard free energies of solvation of the oxidized and reduced species, respectively. The optimized geometries of all species obtained at B3LYP/6-31G(d,p) level of theory were used to determine the absolute thermochemical properties by the frequency calculations under the same level at 298.15 K and 1.00 atm. The results obtained were employed to calculate the quantities $\Delta G^o(g)$, $\Delta G^o(solv,Ox)$, and $\Delta G^o(solv,Red)$. The standard free energy of the free electron was determined by considering its energy (3.720 kJ mol^{-1}) and entropy (0.023 J $mol^{-1}K^{-1}$) at 298 K [33]. Additionally, an adjusted value for the change in the standard state of reactions from one atmosphere in the gas phase to 1 mol l^{-1} in solution should be taken into account for each component as 1.9 kcal mol^{-1}. To establish a consistent electrochemical scale, the absolute values for the oxidation potential obtained from Eq. (2)

were compared with the Hg/Hg_2Cl_2 reference electrode (as known that the saturated calomel electrode), which has an electrode potential value of 4.522 V in non-aqueous solution. The calculated oxidation potential values for oligo(Py)s and the available experimental data in the THF solvent [34] were compiled in Table 5.

Table 5. Calculated oxidation potentials and available experimental values (in V *vs*. Hg/Hg_2Cl_2) [34] for oligo(Py)s in THF.

Oligo(Py)s	E_{ox} (cal.)	E_{ox} (exp.)
di(Py)	0.597	0.60
tri(Py)	0.299	0.28
tet(Py)	0.124	0.16
pen(Py)	0.043	-
hex(Py)	0.007	-
hep(Py)	-0.053	-
oct(Py)	-0.050	-

According to Table 5, the calculated E_{ox} values show an expected decrease with increase in the π-conjugated length of oligo(Py) chains. Furthermore, one can find a qualitative agreement between the predicted E_{ox} values and the available experimental measurements for the short oligomers di-, tri-, and tet(Py). The observed trend in the reduction of E_{ox} for the long oligo(Py) chains is expected with the potential shifting to anodic region with respect to short oligo(Py) chain. The average absolute deviation (AAD) between the predicted and experimental quantities was found to be 0.016 V, which is nice results for oligo(Py)s reported by the proposed theoretical approach. It may conclude that the theoretical protocol used is adequate and valid for predicting the redox potential of the oligo(Py)s.

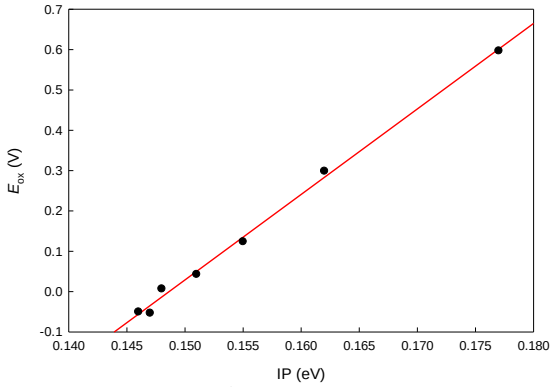

Fig. 5. Correlation plot of the calculated E_{ox} (V) against the IP values in THF.

In Fig. 5, the values for E_{ox} of oligo(Py)s plotted versus the ionization potential in the THF solvent. As illustrated in this figure, there exists a clear linear correlation between the E_{ox} values and the IP values. A straightforward linear relationship has been identified, as demonstrated by the following expression, which establishes a correlation between the E_{ox} and IP values for the oligo(Py) in the THF solution:

$$E_{ox}\ (V) = -3.15 - 21.19\ IP\ (eV) \quad (4)$$

where the correlation coefficient, denoted as r^2, yielded a value of 0.9963. The observed correlation indicates that a higher escaping tendency of electrons corresponding to a low E_{ox} value, be consistent to less positive IP, due to the higher π-conjugation. The correlation obtained provided a resonance effect on the electronic and energetic properties of oligo(Py)s, and thereby, as an evidence for the accuracy of the theoretical approach used.

The relationship between the redox potentials and the energy levels of HOMO has been established by several authors [35, 36]. In this context (Fig. 6), a straightforward linear correlation was discovered, expressed as follows, between the E_{ox} values and the energies of the HOMO levels (E_{HOMO}) for the oligo(Py)s:

$$E_{ox}(V) = -3.48 - 22.74\ E_{HOMO}\ (eV) \quad (5)$$

It is worth noting that the correlation coefficient was determined to be r^2 = 0.9981. This well-known

correlation between the oxidation potential and energy of the highest occupied molecular orbital of oligo(Py)s is to be expected, as oligomers with lower HOMO energy exhibit a greater propensity for electron loss.

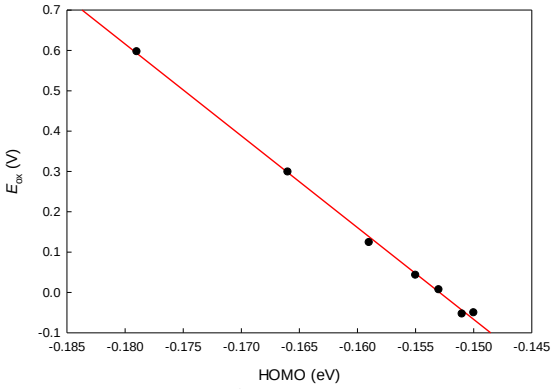

Fig. 6. Correlation plot of the calculated E_{ox} (V) against the HOMO energy (eV) in THF.

In Fig. 7, the E_{ox} values for the oligo(Py)s is plotted against the number of repeating units. According to this figure, the E_{ox} values decrease exponentially as one shifts from 2 to 8 repeating units, related to a less energy barrier for the hole injection for a long oligomer chain. The data was utilized the *Meier* expression, which has been effectively employed to elucidate the absorption and fluorescence values of polymers as the oligomer chain grows [37]. In order to consider the saturation in the infinite chain length limit, as $n \rightarrow \infty$, we employed the following equation:

$$E_{ox}(n) = E_{ox}(\infty) + [E_{ox}(1) - E_{ox}(\infty)] \exp(-a.(n-1)) \quad (6)$$

where a parameter corresponds to the fitting parameter, $E_{ox}(1)$ and $E_{ox}(\infty)$ are the oxidation potentials for the monomer and polymer units, respectively. The use of the *Meier* equation allows us to predict the oxidation potential for the π-conjugated polymeric material. In the case of THF solution, the extrapolated $E_{ox}(\infty)$ for poly(Py) was found to be 0.21 V with the correlation coefficient r^2 = 0.9985. A lower value for the E_{ox} of poly(Py) respect with the initial monomer (1.51 V) suggests a higher charge mobility rate in polymer possibly caused by an increase of the resonance system. It is interesting that the observed trend for the $E_{ox}(\infty)$ value is in good agreement with the experimentally observed potential oxidation of the conducting polymers [38].

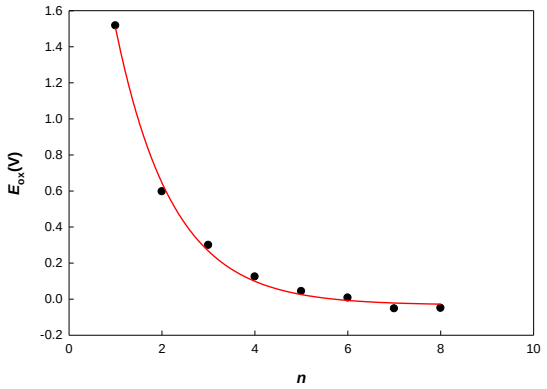

Fig. 7. The oxidation potential of oligo (Py) against the number of repeating units in THF.

3.4. The simulated current-voltage curves (IVs)

Fig. 8 displays IV-curves for a Py monomer and two different short oligo(Py)s obtained by means of simulated electrode device in ATK-DFT software According to Fig. 8, the conductivity of oligo(Py)s significantly increased with respect to monomer. The simulation results reveal that extended conjugated π-electron through the oligomer chain is responsible for the change in the charge carrier's concentration in the studied molecules. An increase in the flow of electric current for both di(Py) and tri(Py) species, indicating that conductivity increased as the number of building units (n) increased.

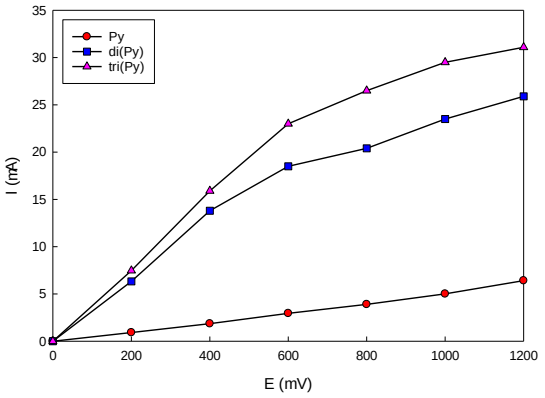

Fig. 8. Simulated current-voltage (IV) curves for Py monomer (-●-), di(Py) (-■-), and tri(Py) (-▲-).

3.5. Analysis of UV-visible spectra

It is evident that comprehending the low-energy excited states of oligomers is crucial for identifying suitable candidates for the production of conducting polymers. To qualitatively evaluate the elucidation of charge-transfer mechanisms in such materials, examining the excited states through TD-DFT calculations proves to be an appropriate approach. We calculated the UV-visible spectra properties including the excitation energies (E_g) and longest wavelengths (λ_{max}) of the maximum absorption peak for each oligo(Py) using TD-DFT with B3LYP/6-31G(d,p) level of theory, which presented in Table 6. According to this table, the λ_{max} values for both the ground and oxidized states increase as one shifts from the dimer to octamer chain.

The maximum peak of simulated absorption spectra for each oligo(Py) in its ground state was depicted in Fig. 9(a). Increasing toward higher wavelength shows that delocalization in aromatic rings of the long oligomer is higher as compared to the short ones, providing a clue that electrical conductivity of the final polymer will be raise as compared to its oligomers. As one can see in Table 6, the oxidation process of oligo(Py)s (Scheme 1) exhibits an evident bathochromic shift and a decrease in the excitation energies with growth of oligomer chain. For instance, in the case of the ground state pen(Py), the calculated λ_{max} value is found to be 388 nm, in contrast, in the oxidized state is found to be 499 nm which is red shifted by 111 nm. The observed trend is comparable to those obtained for the HOMO-LUMO gap energies (Section 3.2).

Table 6. Calculated E_g(eV) and λ_{max}(nm) of simulated absorption spectra for the ground and oxidized states of oligo(Py)s in THF.

	Ground state		Oxidized state	
Oligo(Py)s	E_g	λ_{max}	E_g	λ_{max}
di(Py)	4.68	265	3.84	323
tri(Py)	3.88	319	3.11	399
tet(Py)	3.46	358	2.74	453
pen(Py)	3.19	388	2.48	499
hex(Py)	3.03	409	2.35	528
hep(Py)	2.57	482	2.29	542
oct(Py)	2.51	494	2.22	557

The peak of the maximum absorption of the ground state pen(Py) in the gas phase and both the water and THF solvents were also compared in Fig. 9(b). As can be noted, the solvent effect is more favorable in both the aqueous and non-aqueous solutions, which the excitation energy for pen(Py) in both solutions is red shifted by about 20 nm with respect to one in the gas phase. According to Fig. 9(b), no considerable difference is observed for the excitation energy of pen(Py) in both the water and THF solvents. Generally, it is foreseeable that the utilization of a polymer comprising Py monomer may prove advantageous in the development of a collection of altered compounds possessing desirable characteristics and proficient conduction of electrical charges in the emerging field of opto-electronics.

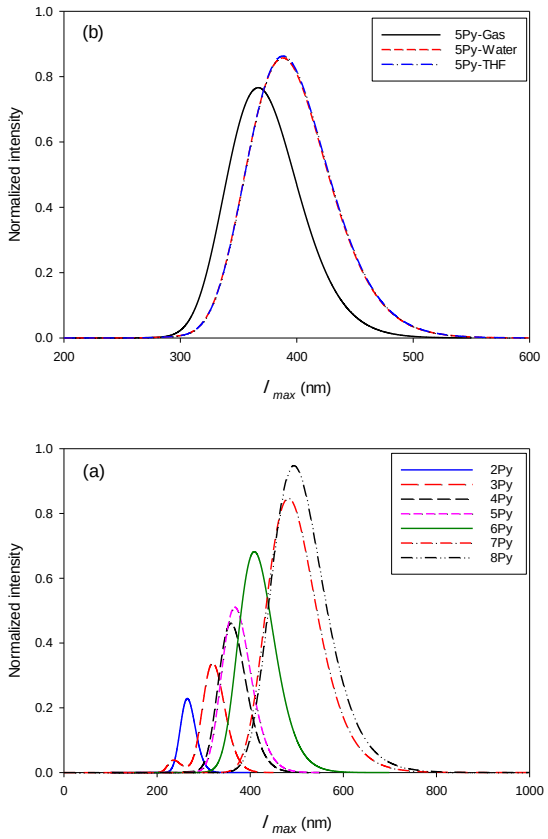

Fig. 9. UV-visible spectra properties obtained at TD/B3LYP/6-31G(d,p) level for: (a) oligo(Py)s in the ground states, and (b) pen(Py) in the gas and both condensed phases.

4. Conclusions

In this work, the DFT-B3LYP/6-31G(d,p) level of theory was employed to calculate the accurate oxidation potentials of a series of oligo(Py)s and final polymer in the gas and condensed phases. The computational study was focused on the exploration of theoretical protocol based on a thermodynamic cycle for the prediction of oxidation potential using the calculated structural and electronic properties of the title oligomers. It is found that the electronic delocalization corresponds to an increase in the aromatic character along the conjugated oligomer chain played fine-tune effects on the structural, electronic, and electro-chemical properties of oligo(Py)s. The electro-chemical polymerization of Py was carried out by means of CV measurements. It was found that the oxidation potential was reduced when the growth of poly(Py) enhanced. Comparison of the calculated results for the oxidation potential of oligo(Py)s with experimental measurements showed a nice agreement with an average absolute deviation 0.016 V. A good correlation was obtained between the oxidation potential and both the ionization potential and HOMO energy. To predict the E_{ox} value for poly(Py), a Meier expression was used to fit the E_{ox} with the length of oligo(Py) chains, which the extrapolated value for poly(Py) was found to be 0.21 V vs. Hg/Hg_2Cl_2 in the THF solvent. A significant difference between the simulated IV-curves of oligomeric products and monomer was observed, in which the electrical conductivity increase with increase building units. Moreover, the outcomes derived from the UV-visible absorption spectra validated the fact that the oxidized entities exhibited reduced excitation energies when compared to their ground states, which coincided well with the estimations made based on the HOMO-LUMO energy gap.

Acknowledgments

The authors express their gratitude to the Shahrood University of Technology for providing financial assistance.

Institutional Review Board Statement

Not applicable.

Informed Consent Statement

Not applicable.

Conflicts of interest

The authors declare that they have no conflicts of interest.

References

[1] Chiang, C.K., Fincher, C.R., Park, Y.W., Heeger, A.J., Shirakawa, H., Louis, F. J., Gau, S.C., & MacDiarmid, A.G., (1978). Electrical conductivity in doped polyacetylene. *Phys. Rev. Lett.*, 40, 1472.

[2] Heremans, P., Cheyns, D., & Rand, B.P., (2009). Strategies for increasing the efficiency of heterojunction organic solar cells: Material

selection and device architecture. *Acc. Chem. Res.*, 42, 1740-1747.

[3] Sheibani, E., Moslempoor, M., & Ghiasabadi, M. (2024). Synthesis and Application of Organic Hole Transporting Materials for Perovskite Solar Cells at Doped-Free Condition. *Applied Chemistry Today*, (71)19, 95-110. (in Persian)

[4] Peng, H., Weng, W., Sun, X., & Fang, X., (2017). Polymer Materials for Energy and Electronic Applications. 1st Edition, Amsterdam: Elsevier, 243-285.

[5] Kasa, T., & Gebrewold, F., (2017). Polymers and its application in light emitting diodes: A review article. *Adv. Phys. Theo. Appl.*, 62, 28-37.

[6] Kulhanek, J., & Bures, F., (2012). Imidazole as a parent π-conjugated backbone in charge-transfer chromophores. *Beilstein J. Org. Chem.*, 8, 25-49.

[7] Lu, M., Zhu, Y., Ma, K., Cao, L., & Wang, K., (2012) Facile synthesis and photo-physical properties of cyano-substituted styryl derivatives based on carbazole/phenothiazine. *Spectrochim. Acta* A, 95, 128-134.

[8] Dunst, K., Karczewski, J., & Jasiński, P., (2017). Nitrogen dioxide sensing properties of PEDOT polymer films. *Sens. Actuators* B, 247, 108-113.

[9] Armitage, B.I., Murugappan, K. Lefferts, M.J., Cowsik, A., & Castell, M.R., (2020). Conducting polymer percolation gas sensor on a flexible substrate. *J. Matr. Chem.* C, 8, 12669-12676.

[10] Liu, X., Zheng, W., Kumar, R., Kumar, M., & Zhang, J., (2022). Conducting polymer-based nanostructures for gas sensors. *Cord. Chem. Rev.*, 462, 214517.

[11] Yao, Z., Wang, J., & Huang, J.P., (2021). High-performance polymer field-effect transistors: from the perspective of multi-level microstructures. *Chem Sci.*, 12, 1193-1205.

[12] Google (2024). Google terms of service. Available at: https://www.nobelprize.org/prizes/chemistry/2000/8961-the-nobel-prize-in-chemistry-2000.

[13] Peng, H., Zhang, L., Soeller, C., & Sejdic, J.T., (2009). Conducting polymers for electrochemical DNA sensing. *Biomaterials*, 30, 2132-2148.

[14] Thunyakontirakun, W., Sriwichai, S., Phanichphant, S., & Janmanee, R., (2019). Fabrication of poly(pyrrole-3-carboxylic acid)/graphene oxide composite thin film for glucose biosensor. *Materials Today: Proceedings*, 17, 2070-2077.

[15] Funt, B.L., & Diaz, A.F., (1991). *Organic electrochemistry: An introduction and a Guide*. New York, Marcel Dekker, p.1337.

[16] Izutsu, K., (2002). *Electrochemistry in nonaqueous solutions*. Wiley-VCH Verlag GmbH & Co. KGaA, pp. 85-106.

[17] Beiginejad, H., Paziresh, S., & Malekpoor, S. (2021). Experimental and theoretical study of hydrolysis for some oxidized urazoles. *Journal of Applied Chemistry*, (60)16, 139-152. (in Persian)

[18] Nikoofard, H., Sargolzaei, M., Kia, B., & Amin, A.H., (2016). DFT study of conjugational electronic structure of aminoalkyl end-capped oligothiophenes up to octamer. *C.R. Chimie*, 19, 646-653.

[19] Pashaei, S., & Hosseinzadeh, S. (2023). Synthesis and investigation of polypyrrole/pomegranate peel powder composites and application for removal of heavy metals from water. *Journal of Applied Chemistry*, (68)18, 63-82. (in Persian)

[20] Rasouli, E., Rahimnejad, M., & Ezoji, H. (2024). Electrochemical determination of dopamine at the surface of carbon oaste electrode modified with the nanocomposite of Ni-MWCNT and titanium dioxide nanoparticles. *Applied Chemistry Today*, (70)19, 293-312. (in Persian)

[21] Baseden, K.A., & Tye, J.W., (2014). Introduction to density functional theory: Calculations by hand on the helium atom. *J. Chem. Educ.*, 91, 2116-2123.

[22] Parvarinezhad, S., & Salehi, M., (2023). New pyrazolone-based Schiff base Cu(II) complexes: Synthesis, spectra, theoretical calculation and protein binding. *Applied Chemistry Today*, (69)18, 113-136. (in Persian)

[23] Frisch, M.J., Trucks, G.W., Schlegel, H.B., et al. (2009). *Gaussian 09W*. Gaussian Inc., Pittsburgh PA.

[24] Cossi, M., Rega, N., Scalmani, G., & Barone, V., (2003). Energies, structures, and electronic properties of molecules in solution with the C-PCM solvation model. *J. Comput. Chem.*, 24, 669-681.

[25] Jacquemin, D., Perpete, E.A., Ciofini, I., & Adamo, C., (2009). Accurate simulation of optical properties in dyes. *Acc. Chem. Res.*, 42, 326-334.

[26] QuantumATK-Semiconductor Modelling, Google (2024). Google terms of service. Available at: https://www.synopsys.com/manufacturing/quantumatk/semiconductor-modeling.html.

[27] QuantumATK V-2023.12 Documentation, Google (2024). Google terms of service. Available at: https://docs.quantumwise.com/manuals/DFTLCAO.html.

[28] Zhang, G., Zhang, H., Li, D., Chen, D., Yu, X., Liu, B., & Li, Z., (2008). End-substitution effect on the geometry and electronic structure of oligoheterocyclics. *Theo. Chem. Account*, 121, 109-122.

[29] Chen, S. & Kar, T., (2012). Theoretical investigation of inhibition efficiencies of some schiff bases as corrosion inhibitors of aluminum. *Int. J. Electrochem. Sci.*, 7, 6265-6275.

30. Camurlu, P., (2014). Polypyrrole derivatives for electrochromic applications. *RSC Adv.*, 4, 55832-5845.

[31] Sadki, S., Scottland, P., Brodie, N., & Sabouraud, G., (2000). The mechanisms of pyrrole electropolymerization. *Chem. Soc. Rev.*, 29, 283-293.

[32] Riahi, S., Eynollahi, S., & Ganjali, M.R., (2009). Parameterization and determination of the electrode potentials of levodopa: Computational study. *Int. J. Electrochem. Sci.*, 4, 551-561.

[33] Bartmess, J.E., (1994). Thermodynamics of the electron and the proton. *J. Phys. Chem.*, 98, 6420-6424.

[34] Andrieux, C.P., & Hapio, P., (1997). Substituent effects on the electrochemical properties of pyrroles and small oligopyrroles. *Chem. Mater*., 9, 723-729.

[35] Dance, I., (2006). The correlation of redox potential, HOMO energy, and oxidation state in metal sulfide clusters and its application to determine the redox level of the FeMo-co active-site cluster of nitrogenase. *Inorg. Chem.*, 45, 5084-5091.

[36] Heffner, J.E., Raber, J.C., Moe, O.A., & Wigal, C.T., (1998). Using cyclic voltammetry and molecular modeling to determine substituent effects in the one-electron reduction of benzoquinones. *J. Chem. Educ.*, 75, 365-367.

[37] Zirzlmeier, J., Schrettl, S., Brauer, J. C., et al. (2020). Optical gap and fundamental gap of oligoynes and carbine. *Nat. Commun.*, 11, 4797-4800.

[38] Fichou, D., (1999). *Handbook of oligo- and polythiophenes.* New York, Wiley.